Theor Chem Acc (2012) 131:1141
DOI 10.1007/s00214-012-1141-y

REGULAR ARTICLE

The nature of the C–As bonds in arsaalkynes: an atoms in molecules and electron localization function study

Tiziana Marino · Maria C. Michelini · Nino Russo · Emilia Sicilia · Marirosa Toscano

Received: 1 July 2011 / Accepted: 2 September 2011 / Published online: 22 February 2012

Abstract The nature of the C–As bonds present in a series of six neutral and anionic arsaalkynes was investigated. The optimized geometries, vibrational frequencies, and wavefunctions of all the studied species were computed using density functional theory (B3LYP/6-311++*G*(2d,2p)). To understand the bonding characteristics, Atoms in Molecules theory and topological analysis of the electron localization function were used. For comparison, natural bond orbital analysis was also performed. The results suggest that in five of the six studied compounds, the C–As bonds are essentially triple bonds, with similar characteristics to the C–P analogues in phosphaalkynes.

Keywords Arsaalkynes · Phosphaalkynes · Atoms in molecules · Electron localization function · Density functional theory

1 Introduction

The chemistry of multiple bond compounds between group 14 elements and heavier pnictogen atoms has been the subject of substantial study [1–9]. These species are interesting from the synthetic point of view, because of the possibility of obtaining new ligands in coordination chemistry or good precursors in material chemistry. Moreover, formation of multiple bonds by third- and forth-row elements is intriguing from a theoretical point of view. New findings continue to challenge widely accepted rules of bonding. As an example, for a long time, the so-called double bond rule, which establishes that thermally stable multiple bond compounds can be formed only by elements of the second period, was not brought into question. However, after the discovery of the first phosphaalkyne, HCP, by Gier in 1961 [10] and the synthesis in 1981 of the first stable compound involving a heavier element (*t*BuCP) [11], this rule was dismissed and the detailed study of the chemistry and properties of phosphaalkynes became a rich area of research. In spite of the analogies between isoelectronic low-coordinated phosphorus compounds and arsenic compounds, the chemistry of arsaalkynes was not similarly investigated owing to the inherent instability of arsenic compounds, and their inaccessibility by synthetic protocols conventionally used in the preparation of phosphaalkynes. The number of known arsaalkynes is consequently much lower.

The first stable arsaalkyne, whose synthesis and structural characterization was reported in 1986, was Mes*-C≡As (Mes* = 2,4,6-tri-*tert*-butylphenyl) [12]. The presence of the bulky Mes* group is mainly responsible for the thermal stability of this compound. Further stabilization effects could come from the interaction of the C≡As triple bond with the aryl π system. Subsequent studies showed that when the less bulky tert-butyl group is employed, the resulting arsaalkyne has only a transient existence [13]. Treatment of a platinum complex with Mes*C≡As resulted in the synthesis of an arsaalkyne-transition metal complex $Pt(PPh_3)_2\{\eta^2 \equiv AsCMes^*\}$ that was structurally

Dedicated to Professor Vincenzo Barone and published as part of the special collection of articles celebrating his 60th birthday.

Electronic supplementary material The online version of this article (doi:10.1007/s00214-012-1141-y) contains supplementary material, which is available to authorized users.

T. Marino · M. C. Michelini · N. Russo (✉) · E. Sicilia · M. Toscano
Dipartimento di Chimica, Università della Calabria, 87030 Arcavacata di Rende, Italy
e-mail: nrusso@unical.it

characterized by X-ray spectroscopy [14] together with the same arsaalkyne Mes*C≡As ligand. More recently, an unexpectedly stable C≡As anionic compound, $[(CF_3)_3BCAs]^-$, was synthesized and characterized together with its lighter congener $[(CF_3)_3BCP]^-$ [15]. Thermally unstable Me–C≡As decomposes well below room temperature [16]; the parent methylidynearsine HC≡As, the third known unsubstitued heteroalkyne, was only very recently synthesized and characterized by mass spectrometry and UV-photoelectron spectroscopy [17].

Theoretical studies of some of the above-mentioned compounds containing a C≡As triple bond have been previously reported. The first theoretical investigation of methylidynearsine HC≡As dates back to 1984 and deals with the theoretical estimation of the gas-phase basicity of molecules having a C–As multiple bond [18]. Geometrical structures of Me–C≡As, and its N and P analogues, were optimized at MP2 level using the LANL1DZ basis set [16]. Mó and collaborators reported the results of a combined theoretical and experimental study of gas-phase acidity of H–C≡As and Me–C≡As and phosphorus-containing analogues [19]. More recently, several theoretical approaches were employed to evaluate the methylidynearsine ionization potential [17]. Electronic and structural properties of neutral, cationic, and anionic methylidynearsine were examined at QCISD, MP2, and B3LYP levels with the 6-311++G** basis set [20]. In a recent study, the vibrational spectrum of HC≡As was calculated using DFT, including anharmonic corrections [21].

We present here a theoretical investigation aimed to gain insight into the nature of C–As bonds in a series of neutral and anionic arsaalkynes. Different bonding analysis methodologies were used, and the obtained bond descriptions are compared. Comparison is made of the present results with previously reported studies [22] of the C–P bonds of phosphaalkynes.

2 Computational methods

The geometries of neutral and anionic species were fully optimized, and all stationary points were characterized by harmonic frequency analysis. The B3LYP hybrid functional [23, 24] was employed with the 6-311++*G*(2d,2p) basis sets, as implemented in Gaussian03 package [25]. In the case of Pt, the LanL2DZ effective core potential [26] was used with its split valence basis sets. The wavefunctions of all optimized structures were obtained at the same level of theory.

Two different topological methodologies were used: the Atoms in Molecules (AIM) theory and analysis of the electron localization function (ELF). The AIM theory is based on the topological analysis of the electron density, $\rho(r)$ [27]. Bonds are defined by a bond path, which is necessary for chemical bonding regardless of its nature. The chemical nature of the bonding may be characterized and classified according to the properties of the bond critical points (BCPs). Topologically, a BCP corresponds to a point in the real space where the gradient of the density, $\nabla\rho_{BCP}$, is zero and where the curvature of ρ_{BCP}, expressed through the three eigenvalues of the diagonalized Hessian of ρ_{BCP}, is positive for an eigenvector linking two atomic centers (λ_3) and negative for the two others (λ_1, λ_2) perpendicular to it. A chemical bond thus results from the competition of the parallel expansion of ρ, which separates charges in their respective atomic basins (λ_3) and the perpendicular contraction of ρ toward a bond path (λ_1, λ_2). The dominant effect is measured by the Laplacian of ρ_{BCP}, $\nabla^2\rho_{BCP}$. Values of ρ_{BCP} greater than 0.2 are typical of covalent bonds, and $\nabla^2\rho_{BCP}$ is generally less than zero for such interactions, reflecting the concentration of electron density along the bond path linking the bonded atoms. Thus, when $\nabla^2\rho_{BCP} < 0$, charge is concentrated at the critical point, while when $\nabla^2\rho_{BCP} > 0$, charge is locally depleted. In strongly polar bonding, there is a significant accumulation of electron density between the nuclei, as in all shared interactions, but the Laplacian can be of either sign.

Additional information of the chemical bond can be obtained through energetic considerations related to the interplay of changes in the potential and kinetic energies. This can be done by applying the local expression of the virial theorem to the critical point, $1/2\nabla^2\rho_{BCP} = 2G_{BCP} + V_{BCP}$, where G_{BCP} and V_{BCP} are the kinetic and potential energy densities at the BCP, respectively [28]. Cremer and Kraka demonstrated that the sign of the total energy, $H_{BPC} = G_{BCP} + V_{BCP}$, is an index of the amount of covalency in the chemical interaction [28, 29]. H_{BCP} is negative for interactions with significant sharing of electrons.

Two other bond properties are usually analyzed in the framework of AIM analysis when the interest is focused on the multiplicity of the bonds, that is, the delocalization index and the ellipticity. The delocalization index, δ(A,B), accounts for the electrons delocalized or shared between the atomic basins of atoms A and B. For bonded atoms, δ(A,B) yields a measure of the bond order between them [30, 31]. A simple relationship between the delocalization index and the formal bond order (number of Lewis bonded pairs) has been found for molecular bonds with equally shared pairs. For polar bonds, there is no longer such a simple relationship. Instead, it has been reported that the delocalization index tends to decrease with the increased electronegativity difference of the atoms involved in the bond [32]. The ellipticity, ε, measures the extent to which density is preferentially accumulated in a given plane

containing the bond path [33–35]. The ellipticity is defined as $\varepsilon = \lambda_1/\lambda_2 - 1$, where $|\lambda_1| \geq |\lambda_2|$. If $\lambda_1 = \lambda_2$, then $\varepsilon = 0$ and the bond is cylindrically symmetric. Values of ε greater than zero indicate partial π-character in a bond or electronic distortion away from σ-symmetry along the path. Double bonds are usually characterized by significant ellipticity values, whereas for triple bonds the bonding regains its cylindrical symmetry resulting in values of ellipticity close to zero [35]. It has been shown that the ellipticity can vary along the bond paths with heteropolar bonds [36]. As a consequence, its value at the BCP could be misleading.

In the present work, the BCPs were analyzed in terms of electron density ρ_{BCP}, its Laplacian $\nabla^2\rho_{BCP}$, and the total energy density at the BCP, H_{BPC}. The delocalization index, δ(C,As), and the ellipticity of the C–As bonds are also reported. AIM calculations were performed using AIMAll [37].

The topological description of the chemical bond proposed by Silvi and Savin [38] is based on the gradient field analysis of the ELF of Becke and Edgecombe [39]. ELF is a scalar function whose gradient field enables to carry out a partition of the molecular space into basins of attractors closely related to electron pair domains of the VSEPR model of molecular geometry [40]. The ELF exhibits maxima at the most probable positions of localized electron pairs, and each maximum is surrounded by a basin in which there is an increased probability of finding an electron pair. These basins correspond to the qualitative electron pair domains of the VSEPR model and have the same geometry as the VSEPR domains [40]. The valence shell of a molecule consists of two types of basin: polysynaptic basins (generally disynaptic), which belong to two atomic valence shells and the monosynaptic ones, which belong to only one valence shell, and which qualitatively correspond to nonbonding valence density. The valence basins are labeled by V followed by a list of the atomic symbols of the centers of the valence shells, that is, V(A) and V(A,B) for a monosynaptic and a disynaptic basin [41]. The electronic population of a synaptic basin, $\bar{N}$, is obtained as the integral of the one-electron density over the basin. The variance of the basin population, $\sigma^2(\bar{N})$, represents the quantum–mechanical uncertainty of the basin population and is a result of the delocalization of electrons [42]. It is also written as the sum of the contributions of all other basins and is used as a normalization factor to represent the cross-contribution between two specific basins. The relative fluctuation of a basin can be expressed as $\lambda = \sigma^2(\bar{N})/\bar{N}$, namely, the variance of the basin normalized for the electronic population [42, 43]. This quantity is very useful to describe the degree of electron delocalization. ELF analysis has provided very useful pieces of information on the bonding for a wide range of chemical cases [44]. ELF analysis was performed using the TopMoD package [45, 46], and the results were visualized with the help of the Molekel 4.3 software [47].

With the aim of comparison, the bonding features of all the studied molecules and the net atomic charges were also analyzed by means of the natural bond orbital (NBO) and the natural population analysis (NPA) [48, 49].

3 Results and discussion

The optimized geometries of the studied molecules are shown in Fig. 1. The computed frequencies of the C–As stretching modes and the carbon and arsenic NPA charges are collected in Table 1.

The dearth of experimental results for compounds containing C–As triple bonds precludes extensive comparison with the computed geometrical and vibrational properties, as was done in our previous study of analogous systems containing a C–P triple bond [22]. The exceptions are $[(CF_3)_3BCAs]^-$ and Mes*CAs; for which geometrical parameters and vibrational frequencies were determined [14, 15]. For all other examined arsaalkynes, no experimental vibrational frequency is available. The present results can, however, be compared with previous theoretical computations for HCAs, CAs^-, and CH_3CAs species [16–21].

The simplest studied species are **(1)** and **(2)** in Fig. 1, in which the C≡As bond lengths are equal to 1.716 and 1.650 Å, respectively. These values are in good agreement with the QCISD/6-311+$G(df,p)$ C≡As bond lengths of 1.724 and 1.658 Å in **(1)** and **(2)**, respectively [19]. Predictably, as a consequence of deprotonation, the charged methylidynearsine species **(1)** has an elongated bond.

In contrast to the unsubstituted compound **(2),** the ethylidynearsine CH_3CAs derivative **(3)** of Fig. 1 has been synthetized [16]. For this species, the C≡As bond distance computed here (1.660 Å) agrees well with the value of 1.658 Å obtained at QCISD/6-311+$G(df,p)$ level [19]. As in the case of analogues with phosphorous, the C≡As bond lengthens from HCAs to CH_3CAs.

Our computed B3LYP vibrational frequencies for the C≡As stretching mode are very similar to previously reported computed values. In particular, for CAs^-, our value of 998 cm^{-1} is very close to that of 983 cm^{-1} previously reported [19]. Analogously, the B3LYP frequencies of 1109 and 1461 cm^{-1} for **(2)** and **(3)** agree well with literature values of 1097 and 1482 cm^{-1}, respectively [19].

The only experimental study of the *t*BuCAs species **(4)** employed it in the synthetic pathway to arsaalkynes, but only as transient species [13]. Our computed geometry of **(4)** is very similar to that obtained for the analogous compound of phosphorous [22]. As expected due to the different sizes of the triply bonded atoms, the C≡As

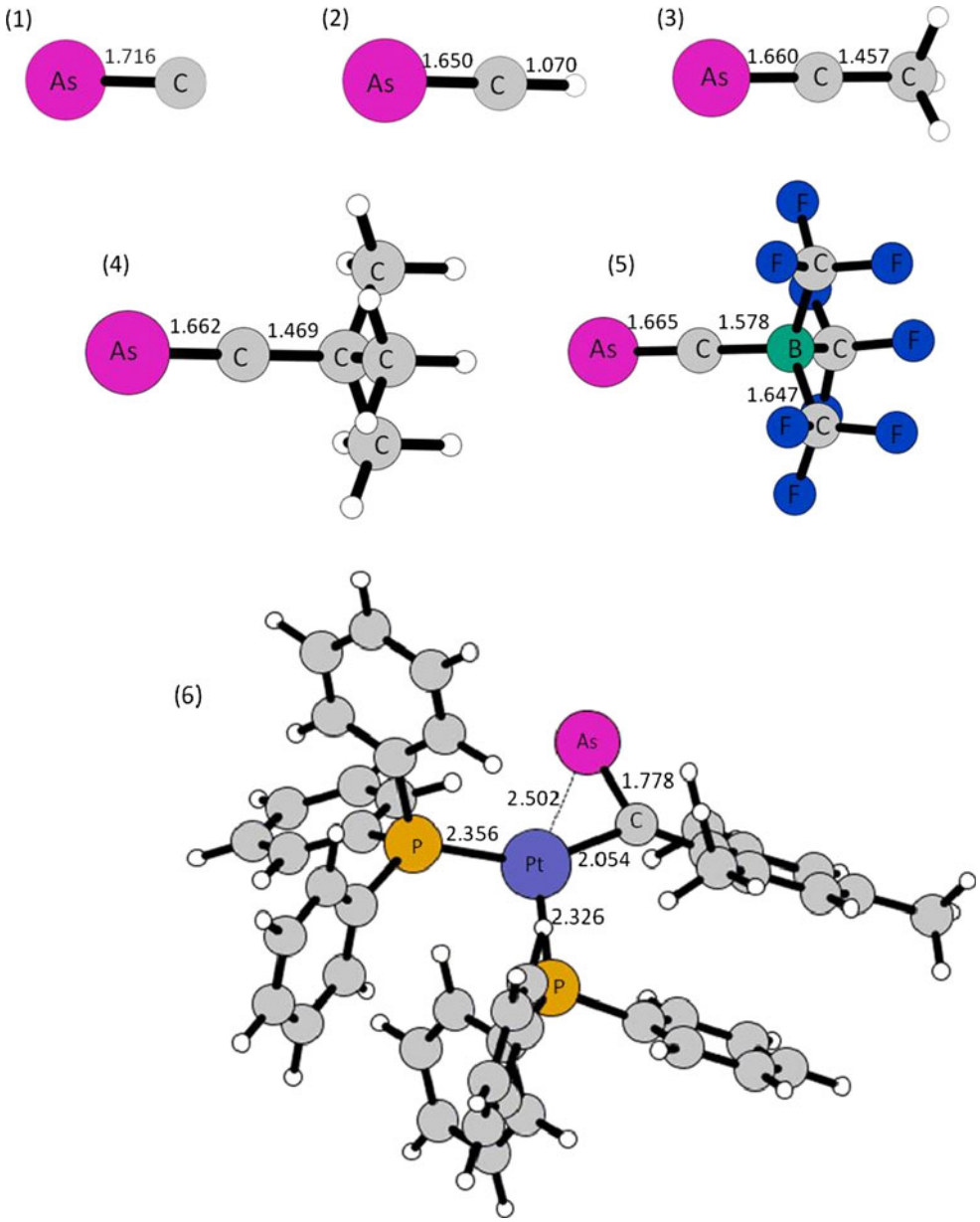

Fig. 1 Selected geometrical parameters of the optimized structures of: (**1**) CAs^-; (**2**) HCAs; (**3**) CH_3CAs; (**4**) *t*BuCAs; (**5**) $[(CF_3)_3BCAs)]^-$; and (**6**) $Pt(PPh_3)_2\{\eta^2\text{-}AsC(C_6H_2Me_3)\}$

Table 1 B3LYP harmonic vibrational frequencies (cm^{-1}) for the C≡As bond stretching and natural atomic charges (|e|) on carbon (qC) and arsenic (qAs) atoms

Species	Frequency	Q_C	Q_{As}
CAs^-	998 (983[a])	−0.84	−0.16
HCAs	1109 (1097[a])	−0.77	0.56
CH_3CAs	1461 (1482[a])	−0.53	0.51
*t*BuCAs	1451	−0.53	0.53
$[(CF_3)_3BCAs)]^-$	1350 (1325[b])	−0.67	0.42
$Pt(PPh_3)_2\{\eta^2\text{-}AsC(C_6H_2Me_3)\}$	–	−0.55	0.43

Available frequency values arising from previous calculations are also reported (in parentheses)

[a] Taken from ref. [19]

[b] Taken from ref. [15]

distance (1.662 Å) is longer than the C≡P distance (1.546 Å). Consequently, the vibrational stretching frequency of the C≡As bond in *t*BuCAs (1451 cm^{-1}) is lower than that of the computed C≡P bond stretch in *t*BuCP (1573 cm^{-1} [22]).

The optimized structure of anionic $[(CF_3)_3BCAs]^-$ ((**5**) in Fig. 1) has much in common with the geometry of species **(4)**. Species (**5**) and the neutral arsaalkyne-transition metal complex (**6**) are examples of kinetically stable anionic arsaalkynes [14, 15]. The computed C–As bond length of 1.665 Å is in good agreement with the measured value of 1.675 Å and is longer (by 0.1 Å) than the computed C–P distance in the corresponding phosphaethynyl compound [22]. The computed B–C–As angle (179.9°) is in accord with the measured value of 177.5°. Finally, the computed stretching frequency (1350 cm^{-1}) agrees very well with the experimental value of 1325 cm^{-1} [14].

The arsaalkyne-transition metal complex (**6**) (Fig. 1) is a simplified model of the Mes*CAs system, which was the first reported stable arsaalkyne compound [12]. The simplified model involves the replacement of tert-butyl with methyl groups. The optimized molecular structure of **(6)** shows that the arsaalkyne bond coordinates the platinum center in a side-on (η^2) fashion. The coordination environment around the metal approximates a square planar structure like that observed in the X-ray crystal structure of Mes*CAs [14]. The computed As≡C bond distance (1.778 Å) and C–C≡As angle (40.0°) are in very good agreement with the experimental values (1.786 Å and 39.5°) [14].

A comparison of the optimized C–As bond lengths of compounds (**1**) to (**5**) (Fig. 1) with the C–P bond distances of analogous compounds [22] indicates a systematic elongation of the bonds between 0.114 and 0.118 Å, when substituting As by P atoms. A slightly larger difference (0.121 Å) is found between the computed C–As distance in (**6**) and the C–P bond length of a similar compound reported in [22].

3.1 AIM bonding analysis

The properties of the electron density at the C–As BCPs of compounds **(1)** to **(6)** are summarized in Table 2. All values of ρ_{BCP} suggest significant concentration of electrons at the bond critical point (c.a. 0.20 a.u.). These values are only slightly lower than the corresponding values for the C–P bonds in analogue species [22]. In all cases, the bond critical points are in regions of positive values of $\nabla^2\rho_{BCP}$ (Table 2).

The computed C–As bond lengths increase in going from compound **(2)** to **(6)** by almost 0.13 Å. The optimized bond distance for CAs^- is 1.716 Å, placing this molecule between **(5)** and **(6)**, according to its C–As bond length. Therefore, the concentration of charge in the bonding region correlates fairly well with the bond length, being lowest for compound **(6)** (d_{C-As} = 1.778 Å) and highest for HCAs (d_{C-As} = 1.650 Å). Compound **(5)** deviates slightly from this trend. In fact, the charge density increases slightly (+0.005 au) with respect to compound **(4)**, despite the small increase in the C–As bond length (+0.003 Å).

The total electronic energy density at the C–As BCP of all the studied species is negative, which indicates that there is significant sharing of electrons despite the positive values of the Laplacian of the density at the same point. There is a good correlation between the amount of charge density and the stabilization energy at the BCP. H_{BCP} is more negative for compound **(2),** which was found to have the highest value of charge density at the BCP, while the lowest absolute value was found for compound (6), which has the lowest ρ_{BCP} (see Table 2).

The delocalization index, δ(C,As), ranges between 2.62 and 2.90 for compounds (**1**) to (**5**) and drops to 1.78 in compound (**6**). The ellipticity of the C–As bonds of compounds (**1**) to (**5**) is very close to zero ($\varepsilon < 10^{-4}$), whereas for compound (**6**) that value rises to 0.05.

It is known that the electron density at the BCP generally shows a good correlation with the bond length and the bond order. However, the actual value of the electron density varies depending on the characteristics of the particular bond that is being analyzed. The main goal of this work has been to give insight into the characteristics of the C–As bonds in a series of compounds presenting formal triple bonds and analyze similarities and differences with similar bonds formed by the lighter members of the group. With this aim, it is useful to perform a comparative analysis of the AIM properties of the bond of interest in a series of compounds. In particular, a set of homologue species containing C–As, C–P, and C–N bonds with different bond orders were chosen as a benchmark. The molecules considered were hydrogen cyanide (HC≡N), methanimine (H_2C=NH), methylamine (H_3C–NH_2), and the corresponding phosphorus and arsenic homologues. The optimized geometries of these molecules are shown in Fig. 2, whereas the computed AIM properties are summarized in Table 3.

An analysis of the results presented in Table 3 shows that in the case of C–N bonds the electron density at the BCP increases by a factor of 1.53 in going from single to double bonds and by a factor of 1.25 in going from double to triple bonds. The same factors drop to 1.29 and 1.15 for C–P bonds and to 1.36 and 1.18 for C–As bonds. Therefore, the reinforcement of the bonds due to the formation of double and triple bonds is notably lower in the case of C–P and C–As bonds. A comparison of the C–N bonds of HC≡N, H_2C=NH, and H_3C–NH_2 with its C–P and C–As homologues shows that the charge density at the C–N

Table 2 AIM topological properties of the C–As bonds of compounds (**1**) to (**6**)

	ρ^{a}_{BCP}	$\nabla^2\rho^{b}_{BCP}$	H^{c}_{BCP}	δ(C,As)[d]	Q_C, Q_{As}[e]
CAs^{-}[f] (**1**)	0.199	0.135	−0.155	2.90	−0.92, −0.08
HCAs (**2**)	0.208	0.385	−0.159	2.76	−0.76, 0.65
CH_3CAs (**3**)	0.203	0.387	−0.152	2.64	−0.72, 0.55
*t*BuCAs (**4**)	0.202	0.379	−0.152	2.62	−0.74, 0.55
$[(CF_3)_3BAsC]^{-}$ (**5**)	0.207	0.331	−0.159	2.72	−1.15, 0.42
$Pt(PPh_3)_2\{\eta^2\text{-}AsC(C_6H_2Me_3)\}$ (**6**)	0.170	0.129	−0.121	1.78	−0.73, 0.31

[a] Electron density at the BCP in a.u.

[b] Laplacian of the electron density at the BCP in a.u.

[c] Total electronic energy density at the C–As BCP

[d] The electron delocalization index, $\boldsymbol{\delta}$(C,As), accounts for the electrons shared between the C and As atoms

[e] AIM atomic charges for the C and As atoms

[f] With the aim of comparison, the corresponding values for CN^{-} are: $\rho_{BCP} = 0.481$, $\nabla^2\rho_{BCP} = -0.770$, δ(C,N) = 2.40, $H_{BCP} = -0.907$, Q_C, $Q_{As} = 0.49, -1.49$. For CP^{-} are: $\rho_{BCP} = 0.213$, $\nabla^2\rho_{BCP} = 0.320$, δ(C,As) = 2.80, $H_{BCP} = -0.219$, Q_C, $Q_{As} = -1.37, 0.37$

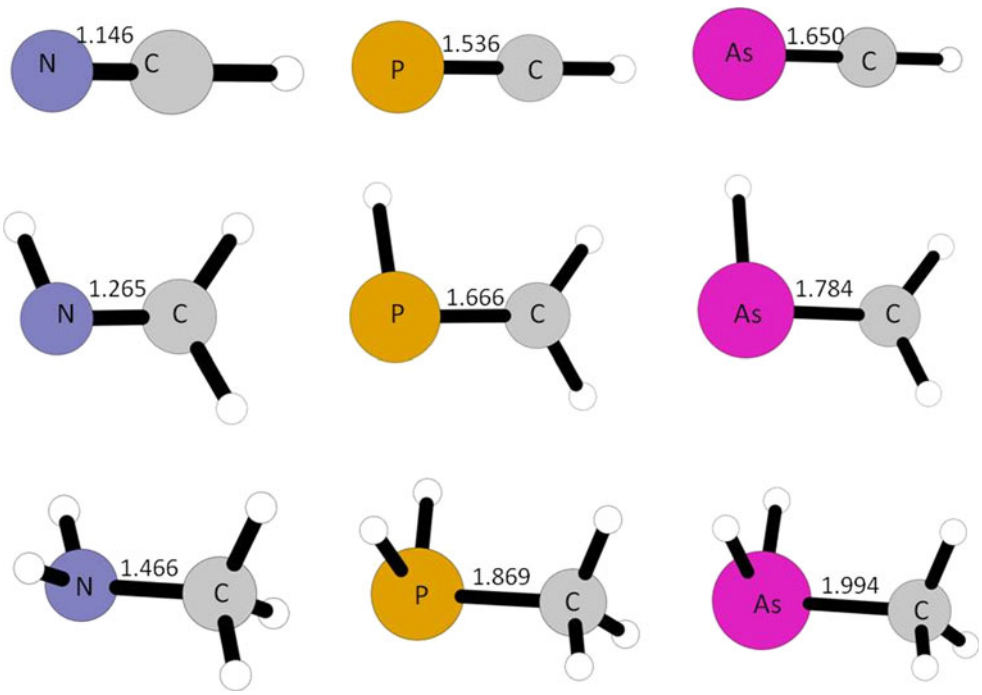

Fig. 2 Optimized C–N, C–P, and C–As bond lengths of: HCN, H_2CNH, and H_3CNH_2 (*first column*); HCP, H_2CPH, and H_3CPH_2 (*second column*) and HCAs, H_2CAsH, and H_3CAsH_2 (*third column*)

BCPs is higher than the same quantity at the C–P bond by a factor of between 1.74 and 2.25 (depending on the order of the bond) and by a factor of between 2.02 and 2.38 for the C–As bond. The difference increases for higher bond orders. The Laplacian of the density at the BCP is negative in all the C–N studied molecules, as well as for the C–P and C–As single bonds of methylphosphine and methylarsine. In contrast, $\nabla^2\rho_{BCP}$ is positive in the case of the double bonds of H_2CPH and H_2CAsH; and the triple bonds of HCP and HCAs. H_{BCP} is negative in all the benchmark molecules, and the amount of this energy correlates fairly well with the charge density at the BCP. As expected, the bond ellipticity reaches a maximum in double bonds, being zero in the case of HCN and its homologues, and close to zero for the single bonded species (less than 0.065). The delocalization index is very close to one (0.93–1.04) for the H_3CXH_2 molecules, between 1.70 and 1.85 for H_2CXH and between 2.56 and 2.76 for HCX (X = N, P, As). The delocalization indices for single, double, and triple bonds for various molecules are reported in literature [50–52]. There is agreement for δ(A,B) to usually be lower than the corresponding bond order. For instance, in C–C bonds, this index takes values of 0.95, 1.89, and 2.85 for single, double, and triple bonds [52]. As previously mentioned, a

Table 3 AIM topological properties of the C–N bonds of HCN, H_2CNH, and H_3CNH_2; C–P bonds of HCP, H_2CPH, and H_3CPH_2; and C–As bonds of HCAs, H_2CAsH, and H_3CAsH_2

	Formal C–N bond order	ρ^{a}_{BCP}	$\nabla^2\rho^{b}_{BCP}$	H^{c}_{BCP}	δ(C,N)[d]	ε[e]	Q_C, Q_N[f]
HCN	3	0.496	−0.325	−0.933	2.60	0.000	0.88, −1.05
H_2CNH	2	0.398	−1.182	−0.649	1.80	0.219	0.67, −1.00
H_3CNH_2	1	0.260	−0.626	−0.252	1.04	0.038	0.36, −0.91
	Formal C–P bond order	ρ^{a}_{BCP}	$\nabla^2\rho^{b}_{BCP}$	H^{d}_{BCP}	δ(C,P)[c]	ε	Q_C, Q^{e}_{P}
HCP	3	0.220	0.634	−0.215	2.56	0.000	−1.17, 1.06
H_2CPH	2	0.192	0.075	−0.195	1.70	0.384	−0.80, 1.19
H_3CPH_2	1	0.149	−0.274	−0.115	0.93	0.061	−0.33, 1.24
	Formal C–As bond order	ρ^{a}_{BCP}	$\nabla^2\rho^{b}_{BCP}$	H^{d}_{BCP}	δ(C,As)[c]	ε	Q_C, Q^{e}_{As}
HCAs	3	0.208	0.385	−0.159	2.76	0.000[g]	−0.76, 0.65
H_2CAsH	2	0.176	0.050	−0.130	1.85	0.263	−0.50, 0.72
H_3CAsH_2	1	0.129	−0.075	−0.073	0.96	0.027	−0.24, 0.81

[a] Electron density at the BCP in a.u.

[b] Laplacian of the electron density at the BCP in a.u.

[c] Total electronic energy density at the BCPs

[d] The electron delocalization index, δ(C,X), accounts for the electrons shared between atoms (X = N, P, and As)

[e] The bond ellipticity

[f] AIM atomic charges for the C, N, P, and As atoms

[g] The actual value is 2.2 10^{-11}

larger departure is expected when the bond pairs are not equally shared between the bonded atoms.

From all the above, some preliminary conclusions that reveal the main electronic characteristics of the C–As bonds in the studied species can be drawn. The C–As bonds of compounds (**1**) to (**6**) show significant concentration of charge density at the BCPs (c.a 0.2 au) together with positive values of $\nabla^2\rho_{BCP}$ and negative values of H_{BCP}. Therefore, despite the charge density is locally depleted in the bonding region, the condition $H_{BCP} < 0$ holds for all the studied bonds, which permits to qualitatively classify those bonds as shared in nature. Despite the known dependency of the delocalization index with the electronegative difference of the bonded atoms, the present results seem to indicate that this index gives a reliable indication of the bond orders for the case under study. According to this index, compounds (**1**) to (**5**) are characterized by the presence of a triple C–As bond, whereas the value of this parameter in compound (**6**) is closer to those characteristic of double bonds (Table 3). The values of ellipticity at the BCPs confirm that compounds (**1**) to (**5**) are cylindrically symmetric. Even when there is an important increase in the ellipticity at the C–As BCP of compound (**6**), the computed value is still out of the range of double bonded C–As bonds (Table 3). Therefore, no definitive conclusions can be drawn on the basis of this index.

In summary, the topological analysis of the charge density indicates that the C–As bonds of compounds (**1**) to (**5**) can be described as triple bonds, weakened by an important depletion of the charge density in the bond region. The C–As bond of compound (**6**) shows some differences with those of compound (**5**), that is, the characteristics of that bond are closer to those of typical C–As double bonds.

3.2 ELF bonding analysis

The main information concerning the C–As bonds of compounds (**1**) to (**6**) obtained by the topological analysis of the ELF function is presented in Table 4. The basin populations of the disynaptic and monosynaptic basins involving the As atoms, V(C,As) and V(As), are reported together with the electronic population of the second disynaptic basin involving the C atom engaged in the C–As bond, V(C,R). The basin variances, $\sigma^2(\bar{N})$, and the relative fluctuations, $\lambda(\bar{N})$, are included in the same table. Figures 3 and 4 show the ELF isosurfaces for compounds (**1**) to (**5**) and (**6**), respectively.

ELF analysis was also performed on the benchmark molecules, namely, HC≡N, H_2C=NH, H_3C–NH_2, and the phosphorus and arsenic analogues. The obtained results are reported in Table 5, whereas the ELF isosurfaces are shown in Fig. 5.

Table 4 ELF topological properties of the C–As bonds of compounds (**1**) to (**6**)

	V(C,As), $\sigma^2(\bar{N})$, $\lambda(\bar{N})$	V(C,R), $\sigma^2(\bar{N})$, $\lambda(\bar{N})$	V(As), $\sigma^2(\bar{N})$, $\lambda(\bar{N})$
CAs^{-}[a] (**1**)	2.82, 1.47, 0.52	2.72, 1.01, 0.37[b]	4.72, 2.10, 0.44
HCAs (**2**)	4.20, 1.72, 0.41	2.31, 0.71, 0.31 (R=H)	3.82, 1.86, 0.49
CH_3CAs (**3**)	3 × 1.46, 3 × 0.94, 0.64	2.14, 1.07, 0.50 (R=C)	3.89, 1.88, 0.48
*t*BuCAs (**4**)	3 × 1.44, 3 × 0.93, 0.65	2.20, 1.10, 0.50 (R=C)	3.94, 1.90, 0.48
$[(CF_3)_3BCAs)]^{-}$ (**5**)	3 × 1.33, 3 × 0.89, 0.67	2.37, 1.11, 0.47 (R=B)	4.04, 1.92, 0.48
$Pt(PPh_3)_2\{\eta^2\text{-}AsC(C_6H_2Me_3)\}$ (**6**)	2.91, 1.56, 0.54	1.64, 1.08, 0.66 (R=Pt)	3.79, 1.96, 0.52
		2.25, 1.11, 0.49 (R=C)	

The basin populations, $\bar{N}$, the variance of the basin populations, $\sigma^2(\bar{N})$, and the relative fluctuation, $\lambda(\bar{N})$, are given in electrons

[a] With the aim of comparison, the corresponding values for CN^{-} are: V(C,N), $\sigma^2(\bar{N})$, $\lambda(\bar{N})$ = 3.39, 1.45, 0.43 and V(N), $\sigma^2(\bar{N})$, $\lambda(\bar{N})$ = 3.54, 1.27, 0.36. For CP^{-} : V(C,P), $\sigma^2(\bar{N})$, $\lambda(\bar{N})$ = 2.91, 1.39, 0.48 and V(P), $\sigma^2(\bar{N})$, $\lambda(\bar{N})$ = 4.22, 1.55, 0.37

[b] This value corresponds to the population and the variance of the monosynaptic V(C) basin

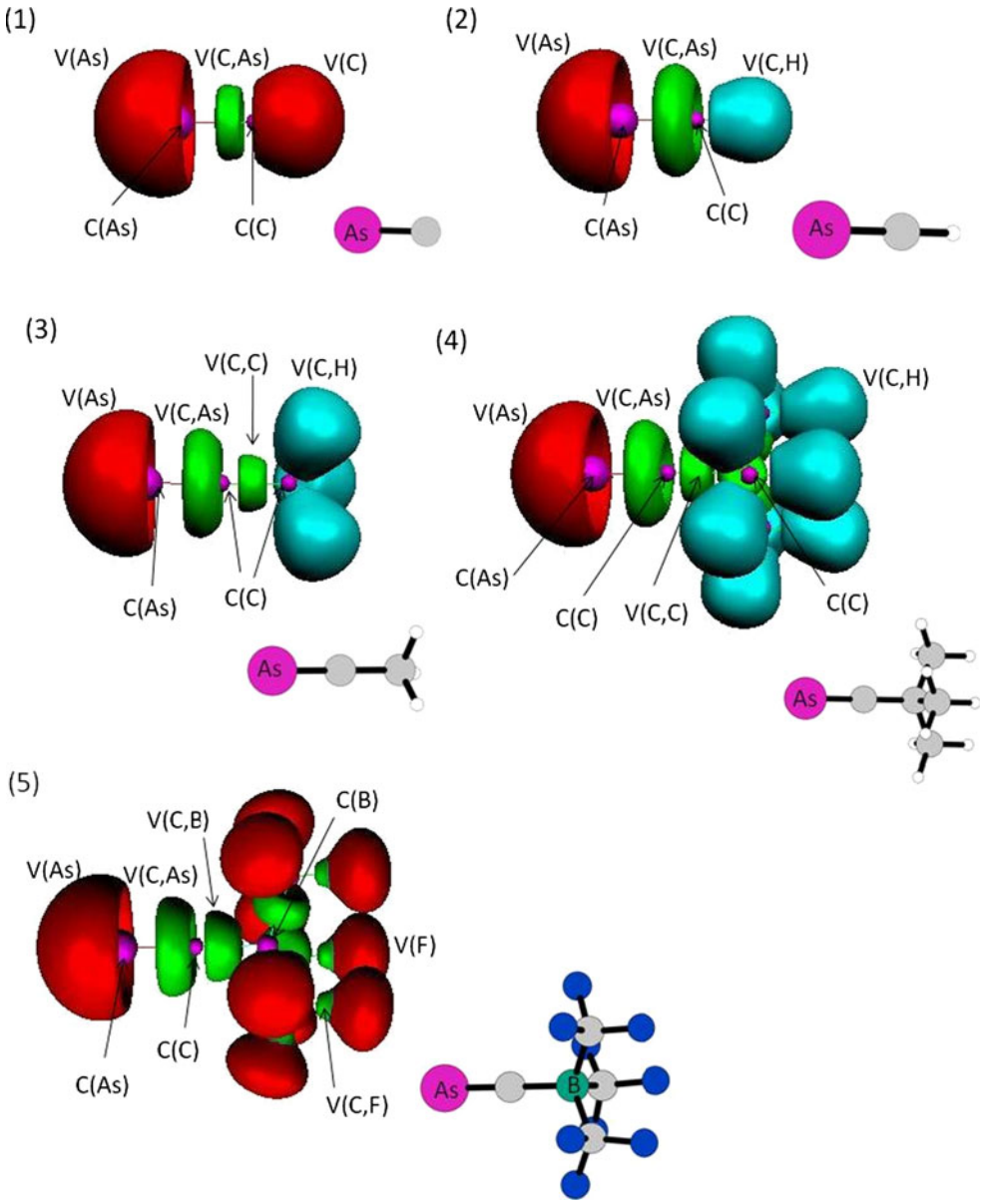

Fig. 3 ELF isosurfaces ($\eta = 0.75$) for optimized structures of: (**1**) CAs^{-}; (**2**) HCAs; (**3**) CH_3CAs; (**4**) *t*BuCAs; and (**5**) $[(CF_3)_3BCAs)]^{-}$. Core basins are represented in *magenta*, valence monosynaptic in *red*, protonated disynaptic in *light blue*, and valence disynaptic in *green*. To help the visualization, *bold* and *sticks* representations of the optimized structures are shown in the *insets*

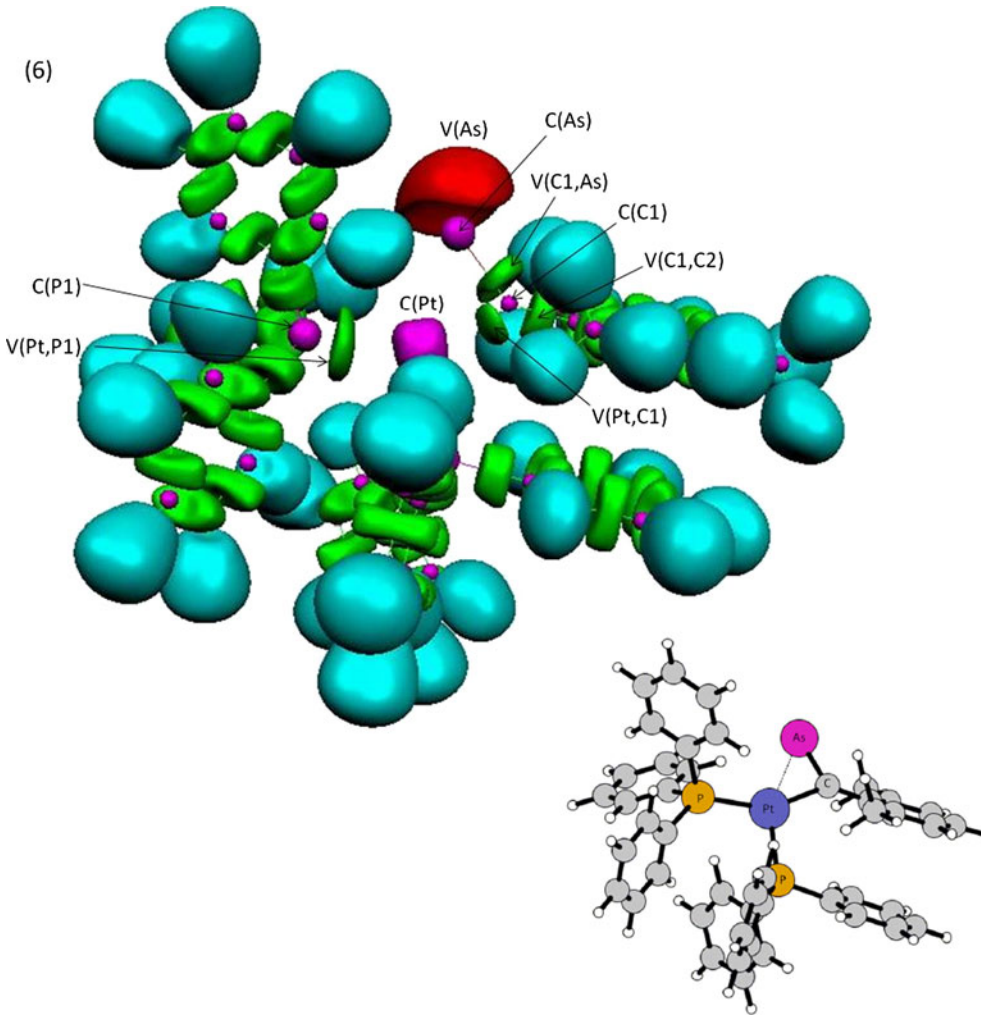

Fig. 4 ELF isosurfaces ($\eta = 0.75$) for the optimized structure of compound (**6**), $Pt(PPh_3)_2\{\eta^2\text{-}AsC(C_6H_2Me_3)\}$. Core basins are represented in *magenta*, valence monosynaptic in *red*, protonated disynaptic in *light blue,* and valence disynaptic in *green*. To help the visualization, a *bold* and *sticks* representation of the optimized structure are shown in the *insets*

Table 5 ELF topological properties of the C–N bonds of HCN, H_2CNH, and H_3CNH_2; C–P bonds of HCP, H_2CPH, and H_3CPH_2; and C–As bonds of HCAs, H_2CAsH, and H_3CAsH_2

	V(C,N), $\sigma^2(\bar{N})$, $\lambda(\bar{N})$	V(N,H), $\sigma^2(\bar{N})$, $\lambda(\bar{N})$	V(N), $\sigma^2(\bar{N})$, $\lambda(\bar{N})$
HCN	4.16, 1.53, 0.37	2.32, 0.68, 0.29[a]	3.32, 1.20, 0.36
H_2CNH	2.93, 1.38, 0.47	1.95, 0.75, 0.38	2.67, 1.08, 0.40
H_3CNH_2	1.65, 0.95, 0.58	1.95, 0.77, 0.39	2.18, 0.99, 0.45
	V(C,P), $\sigma^2(\bar{N})$, $\lambda(\bar{N})$	V(P,H), $\sigma^2(\bar{N})$, $\lambda(\bar{N})$	V(P), $\sigma^2(\bar{N})$, $\lambda(\bar{N})$
HCP	4.08, 1.57, 0.38	2.31, 0.70, 0.30[a]	3.45, 1.34, 0.39
H_2CPH	3.01, 1.38, 0.46	2.03, 0.61, 0.30	2.61, 1.05, 0.40
H_3CPH_2	1.80, 0.98, 0.54	1.99, 0.62, 0.31	2.12, 0.85, 0.40
	V(C,As), $\sigma^2(\bar{N})$, $\lambda(\bar{N})$	V(As,H), $\sigma^2(\bar{N})$, $\lambda(\bar{N})$	V(As), $\sigma^2(\bar{N})$, $\lambda(\bar{N})$
HCAs	4.20, 1.72, 0.41	2.31, 0.71, 0.31[a]	3.82, 1.86, 0.49
H_2CAsH	2 × 1.54, 2 × 0.96, 0.62	2.07, 0.71, 0.34	2.96, 1.46, 0.49
H_3CAsH_2	1.76, 1.03, 0.59	2.03, 0.71, 0.35	2.47, 1.22, 0.49

The basin populations, $\bar{N}$, the variance of the basin populations, $\sigma^2(\bar{N})$, and the relative fluctuation, $\lambda(\bar{N})$, are given in electrons

[a] This value corresponds to the population and the variance of the V(C,H) basin

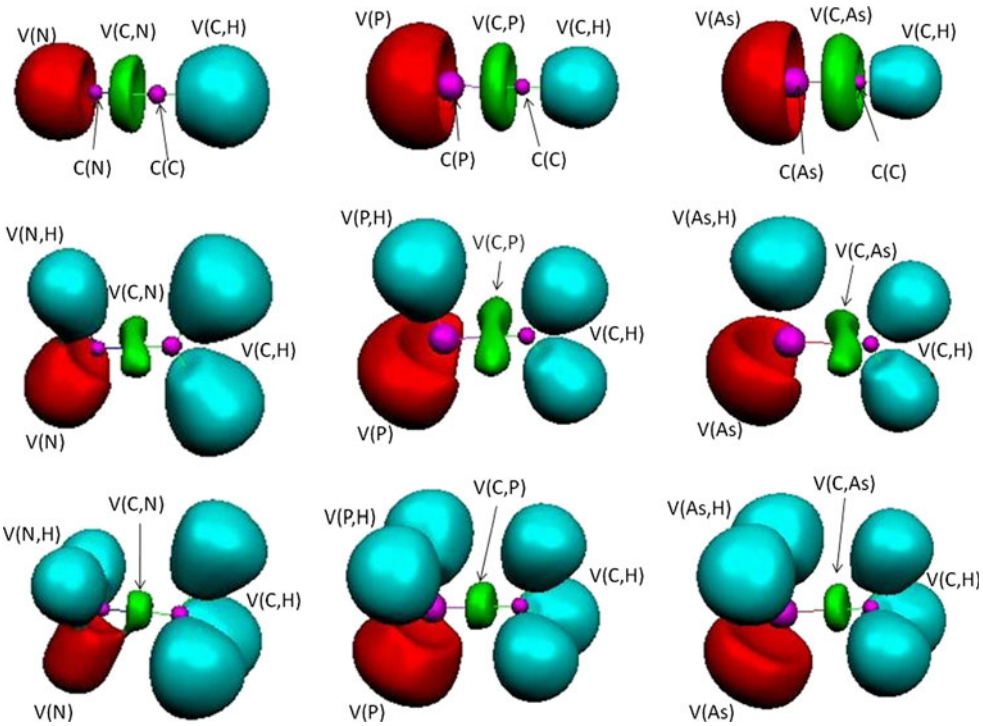

Fig. 5 ELF isosurfaces ($\eta = 0.8$ for *first* and *second column*, 0.75 for *third column*) for optimized structures of: HCN, H_2CNH, and H_3CNH_2 (*first column*); HCP, H_2CPH, and H_3CPH_2 (*second column*) and HCAs, H_2CAsH, and H_3CAsH_2 (*third column*). Core basins are represented in *magenta*, valence monosynaptic in *red*, protonated disynaptic in *light blue,* and valence disynaptic in *green*

A comparison of the ELF results performed on the benchmark molecules (Table 5) shows that from a topological point of view, that is, number and type of basins, there are no qualitative changes when substituting the N atom by P or As. ELF isosurfaces reveal that disynaptic basins resembling prolate spheroids elongated above and below the molecular plane (depicted in green in Fig. 5), which are characteristic of double bonds, for $H_2C{=}NH$ and its phosphorus and arsenic analogues, whereas torus-like disynaptic basins of cylindrical symmetry typical of triple bonds are present in $HC{\equiv}N$ and its homologues. As can be seen in Fig. 5, the disynaptic valence basins are always located closer to the most electronegative atom. The ELF descriptions of HCN, $H_2C{=}NH$, and $H_2C{=}PH$ obtained here agree with the same type of study performed by Chesnut [53].

There is a good correlation between the calculated mean values of the basin populations and the formal bond order. The disynaptic valence electron populations are between 1.65 and 1.80 e^- for formal single bonds, between 2.93 and 3.08 e^- for double, and between 4.08 and 4.20 e^- for triple bonds. There is an important increase in the electron delocalization in going from N to As, as evidenced by the rise in the values of the relative fluctuation of the disynaptic and monosynaptic basins involving those atoms (Table 5). The electron population of the monosynaptic valence basins increases with the increase in the formal bond order, and the highest values involve As atoms. As a consequence of the high monosynaptic electron population, the disynaptic basins representing the triple bonds have an electron population notably lower than the expected six electrons. Previous theoretical studies have shown that this is usually the case in molecules containing triple bonds in the presence of lone pairs, and the effect has been called lone-pair bond weakening effect (LPBWE) [54]. The bonding population has been shown to be usually significantly lower than the expected six electrons, at the expense of increased lone-pair populations [22, 54, 55].

The electron population of the disynaptic *V*(C,As) basins of compounds (**1**) to (**6**) ranges from 2.82 to 4.38 electrons. In all cases, the main atomic contribution to these basins comes from the C atom (between 71 and 77% of the total population). As evidenced in Table 3, three *V*(C,As) basins have been located for CH_3CAs, *t*BuCAs, and $[(CF_3)_3BCAs]^-$, each of them with a basin population of between 1.33 and 1.46 e^-. It is known that generally there is no direct correspondence between the number of valence disynaptic attractors representing the multiple bond in topological analysis of ELF and the multiplicity of the bond. Previous studies have concluded that the multiplicity of disynaptic basins can be better explained by symmetry considerations [44]. As for the benchmark molecules, the monosynaptic *V*(As) basins have electron populations that are much higher than the expected value for a formal single lone pair (2 electrons). Those values range between 3.79 and 4.72 e^-. Both valence basins, *V*(As) and *V*(C,As), are characterized for having very high relative fluctuations (0.41–0.67), which indicates a great degree of electron delocalization.

A comparison of Figs. 3 and 5 puts in evidence the similarity between the torus-like disynaptic *V*(C,As) basins

of compounds (**1**) to (**5**), and the ones present in HC≡N and its homologues. The *V*(C,As) basin of compound (6) departs from the cylindrical symmetry that characterizes the same basin in compounds (**1**) to (**5**) (see Figure S1, Supporting Information for a better view of this basin).

The first studied compound, CAs^-, has special characteristics due to the presence of lone pairs on both bonded atoms. In fact, the disynaptic basin population is the lowest of all the studied compounds, due to the extensive delocalization of the bonding electrons with both monosynaptic valence basins, *V*(C) and *V*(As), which have electronic population notably higher than the expected 2 electrons (Table 4). A comparison of the characteristic of the bonds of CN^-, CP^-, and CAs^- shows an important drop in the electron population of the disynaptic basin involving the two atoms forming the bond, from the 3.39 e^- of CN^- to the 2.82 e^- of CAs^-. This drop is accompanied by an increase in the population of the monosynaptic basins, from the 3.54 e^- of *V*(N) to the 4.72 e^- of *V*(As). As observed in the benchmark molecules, there is also an important increase in the relative fluctuation of the basins, which indicates an increase in electron delocalization between the disynaptic and monosynaptic basins in going from CN^- to CAs^-.

The topological representation obtained from ELF analysis is usually interpreted in terms of superposition of mesomeric structures [56, 57]. Therefore, the valence population can be considered as the result of the weighted contribution of different mesomeric structures of that molecule. Within this interpretation, the trend observed in the disynaptic basin population in going from CN^- to CAs^- indicates that the weight of the mesomeric structure representing a triple bond between the two atoms is less important in the case of CAs^-. ELF analysis, therefore, supports the findings obtained by AIM, according to which there is an important drop of the BCP charge density in going from CN^- to CAs^- (see footnote of Table 2).

There is an important increase in the disynaptic *V*(C,As) basin population in going from CAs^- to HCAs, that is, from 2.82 to 4.20 e^-. As previously mentioned, the depleted *V*(C,As) population is due to the high electron delocalization with the lone pairs of both, C and As atoms.

Compounds (**2**) to (**5**) show very close values of electron population of the *V*(C,As) valence basin, and the small changes observed can be rationalized considering the characteristics of the group bonded to the C atom engaged in the C–As bond. Going from HCAs to CH_3CAs, there is a small increase in the *V*(C,As) electron population, that is, from 4.20 to 4.38 (3×1.46) e^-, which confirms the greater electron-releasing character of the CH_3 group compared with the inductive effect of the H atom. There are not evident changes in the *V*(C,As) population in going from CH_3CAs to *t*BuCAs, despite the expected higher inductive effect of the *tert*-butyl group; but there is an important decrease of basin population in compound (**5**). The strong inductive effect of the electronegative CF_3 groups provokes a depopulation of the *V*(C,As) basin. In $[(CF_3)_3BCAs]^-$, the boron atom in engaged in four covalent bonds with four different carbon atoms, as evidenced by the presence of four disynaptic *V*(C,B) valence basins with electron populations of between 2.20 and 2.37 e^-. The contribution of boron to these valence populations is of only 13%. Therefore, the C atom engaged in the C–As bond contributes importantly to the formation of the B–C bond, and this reduces the availability of charge for the formation of the C–As bond. This is evidenced by the lower contribution of electron charge from that atom to the *V*(C,As) valence basin (74% in contrast to the 77% of compounds (2), (3), and (4)).

Compound (6) has a much lower *V*(C,As) electronic population, 2.91 e^-, with almost 74% of that population coming from the C atom. The torus-like symmetry typical of triple bonds is somewhat lost in the *V*(C,As) valence basin of this compound (see Figure S1, Supporting Information). The C atom engaged in the C–As bond participates also in other two valence basins: one with a second C atom and another with the Pt atom, *V*(C1,Pt), as shown in Fig. 4. Pt is involved in the formation of three valence basins, the previously mentioned *V*(C1,Pt), and two valence basins *V*(Pt,P1) and *V*(Pt,P2) containing a valence population of c.a. 2.22 e^-. In all cases, the contribution of the Pt atom to the total electronic population of the disynaptic basins is very low, that is, 20%.

The bonding description of complex (**6**) obtained by ELF is supported by AIM analysis. In fact, three BCPs involving Pt atom were localized, a Pt–C BCP with a charge density of 0.128 a.u. and two Pt–P BCPs with charge densities of around 0.100 au. In all cases, the Laplacian is positive (between 0.16 and 0.21 a.u.), and the total energy density H_{BCP} is negative.

3.3 NBO analysis

In general, NBO analysis confirms the triple bond nature between C and As atoms in all studied species except (**6**). As an example of a bond analysis, the σ bond and the two π bonds characterizing the *t*BuCAs species derive from the overlap between the hybrid sp and pure p orbitals of the C and As atoms, in accordance with the following composition: $\sigma(CAs) = 0.81(sp)_C + 0.58(sp^{3.33})_{As}$ and $\pi(CAs) = 0.74(p)_C + 0.67(p)_{As}$. In the other structures, the compositions are nearly the same. Similar results have been obtained in the analogues involving the phosphorus atom.

In the case of the complex (**6**), the bonding analysis obtained by NBO is different since the C≡As bond is described as a double bond whose σ- and π-components

arise from the orbital overlaps $0.80(sp^{1.68})_C + 0.59(sp^{5.06})_{As}$ and $0.72(p)_C + 0.68(p)_{As}$, respectively. This result confirms the experimental observation according to which the value of the C–As bond length (1.786 Å) is closer to that predicted for an As=C bond in arsaalkenes. The analogous compound of phosphorus shows, instead, a C–P triple bond [22].

4 Conclusions

In this work, we have attempted to give insight into the nature of the C–As bonds of a series of compounds by means of a comparative analysis of the bonding characteristics, which were analyzed using different methodologies (AIM, ELF, NBO).

The results of the present study can be summarized as follows:

1. According to the topological analysis of the charge density, the C–As bonds of all the studied compounds show a significant concentration of charge at the BCP. All of them are characterized by positive values of the Laplacian of the charge density and negative values of total energy density at the BCP, which indicates that the nature of the bonds can be characterized as shared. An analysis of diverse AIM properties indicates that the C–As bonds of compounds (**1**) to (**5**) can be described as triple bonds weakened by an important depletion of the charge density in the bond region. The studied AIM topological properties seem to indicate that the C–As bond of compound (**6**) has characteristics closer to those of a double bond.
2. The results of ELF analysis support the conclusions drawn from AIM analysis. From a topological point of view, the valence disynaptic basins, which represent that C–As bonds of compounds (**1**) to (**5**), have torus-like shapes, typical of triple bonds. The valence basin electron populations are much lower than the expected value of six electrons due to an important electron delocalization between the disynaptic V(C,As) basins and the monosynaptic valence basins representing the As lone pairs. This type of depleted valence basins has been often found in molecules containing triple bonds in the presence of lone pairs. The disynaptic valence basin representing the C–As bond of complex (**6**) has a more distorted shape, and the valence population is markedly lower than that of compounds (**1**) to (**5**).
3. AIM and ELF topological analyses performed on a series of homologue molecules containing single, double, and triple C–N, C–S, and C–As bonds have permitted evaluation of the bond properties changes that take place when substituting nitrogen atom by its heavier congeners. AIM analysis shows an important decrease of the BCP charge density in going from N to As, especially in the case of triple bonds. The Laplacian of the charge density increases from the large negative values of the C–N bonds to positive values in the case of multiple C–P and C–As bonds. ELF analysis shows that the substitution of N by P or As does not change qualitatively the topological properties of the studied molecules. The main effect of that substitution is an increase in the electron delocalization, which is highest for molecules containing C≡As triple bonds.
4. NBO analysis agrees well with the indications arising from the topological methodologies confirming that C and As atoms are linked together by a triple bond in all the studied species, with the only exception of the compound (**6**).

Acknowledgments We gratefully acknowledge the Dipartimento di Chimica, Università della Calabria for financial aid.

References

1. Barrau J, Esoudié J, Satgé J (1990) Chem Rev 90:283
2. Grev RS (1991) Adv Organomet Chem 33:125
3. Esoudié J, Couret C, Ranaivonjatovo H, Satgé J (1994) Coord Chem Rev 130:427
4. Barrau J, Rima G (1998) Coord Chem Rev 178:593
5. Esoudie' J, Couret C, Ranaivonjatovo H (1998) Coord Chem Rev 178:565
6. Tokitoh N, Matsumoto T, Okazaki R (1999) Bull Chem Soc Jpn 72:1665
7. Power PP (1999) Chem Rev 99:3463
8. Leigh WJ (1999) Pure Appl Chem 71:453
9. Tokitoh N (1999) Pure Appl Chem 71:495
10. Gier TE (1961) J Am Chem Soc 83:1769
11. Becker G, Gresser G, Uhl W (1981) Z Naturforsch B 36:16
12. Märkl G, Sejpka H (1986) Angew Chem Int Ed 25:264
13. Hitchcock PB, Johnson JA, Nixon J F (1993) Angew Chem Int Ed 32:103
14. Hitchcock PB, Johnson JA, Nixon JF J Chem Soc Chem Commun 2061
15. Finze M, Bernhardt E, Willner H, Lehmann CW (2004) Angew Chem Int Ed 43:4160
16. Guillemin JC, Lassalle L, Dréan P, Wlodarczak G, Demaison J (1994) J Am Chem Soc 116:8930
17. Guillemin JC, Chrostowska A, Dargelos A, Nguyen TXM, Graciaa A, Guenot P (2008) Chem Commun 4204
18. Lohr LL, Scheiner AC (1984) THEOCHEM 18:195
19. Mó O, Yanez M, Guillemin JC, Riague EH, Gal JF, Maria PC, Poliart CD (2002) Chem Eur J 8:4919
20. Nazari F, Ansari N (2010) J Mol Model 16:1075
21. Marchal R, Bégué D, Chrostowska A, Pouchan C (2010) Chem Phys Lett 493:24
22. Lucas MF, Michelini MC, Russo N, Sicilia E (2008) J Chem Theory Comput 4:397
23. Becke AD (1993) J Chem Phys 98:5648
24. Stephens PJ, Devlin FJ, Chabalowski CF, Frisch MJ (1994) J Phys Chem 98:11623

25. Frisch MJ, Trucks GW, Schlegel HB, Scuseria GE, Robb MA, Cheeseman JR, Montgomery JA, Jr, Vreven T, Kudin KN, Burant JC, Millam JM, Iyengar SS, Tomasi J, Barone V, Mennucci B, Cossi M, Scalmani G, Rega N, Petersson GA, Nakatsuji H, Hada M, Ehara M, Toyota K, Fukuda R, Hasegawa J, Ishida M, Nakajima T, Honda Y, Kitao O, Nakai H, Klene M, Li X, Knox JE, Hratchian HP, Cross JB, Bakken V, Adamo C, Jaramillo J, Gomperts R, Stratmann RE, Yazyev O, Austin AJ, Cammi R, Pomelli C, Ochterski JW, Ayala PY, Morokuma K, Voth GA, Salvador P, Dannenberg JJ, Zakrzewski VG, Dapprich S, Daniels AD, Strain MC, Farkas O, Malick DK, Rabuck AD, Raghavachari K, Foresman JB, Ortiz JV, Cui Q, Baboul AG, Clifford S, Cioslowski J, Stefanov BB, Liu G, Liashenko A, Piskorz P, Komaromi I, Martin RL, Fox DJ, Keith T, Al-Laham MA, PengCY,Nanayakkara A, ChallacombeM,Gill PMW, Johnson B, Chen W, Wong MW, Gonzalez C, Pople JA (2004) Gaussian Inc., Wallingford
26. Wadt WR, Hay PJ (1985) J Chem Phys 82:284
27. Bader RFW (1990) Atoms in molecules. A quantum theory. Oxford University Press, Oxford
28. Cremer D, Kraka E (1984) Croat Chem Acta 57:1259
29. Cremer D, Kraka E (1984) Angew Chem Int Ed Engl 23:627
30. Fradera X, Austen MA, Bader RFW (1999) J Phys Chem A 103:304
31. Fradera X, Poater J, Simon S, Duran M, Solà M (2002) Theor Chem Acc 108:214
32. Poater J, Duran M, Solà M, Silvi B (2005) Chem Rev 105:3911
33. Cremer D, Kraka E, Slee TS, Bader RFW, Lau CDH, Nguyen-Dang TT, McDougall PJ (1983) J Am Chem Soc 105:5069
34. Bader RFW, Slee TS, Cremer D, Kraka E (1983) J Am Chem Soc 105:5061
35. Schrer W, Sirsch P, Shorokhov DM, Tafipolsky M, McGrady GS, Gullo E (2003) Chem Eur J 9:6057
36. Cheesman JR, Carroll MT, Bader RFW (1988) Chem Phys Lett 143:450
37. Keith TA (2011) AIMAll (Version 11.05.16) (aim.tkgristmill.com)
38. Silvi B, Savin A (1994) Nature 371:683
39. Becke AD, Edgecombe KE (1990) J Chem Phys 92:5397
40. Gillespie RJ, Robinson EA (2007) J Comput Chem 28:87
41. Savin A, Silvi B, Colonna N (1996) Can J Chem 74:1088
42. Noury S, Colonna N, Savin A, Silvi B (1998) J Molec Struct 450:59
43. Silvi B (2004) Phys Chem Chem Phys 6:256
44. Silvi B, Fourré I, Alikhani ME (2005) Monatshefte für Chemie 136:855
45. Noury S, Krokidis X, Fuster F, Silvi B (1997) TopMoD package, Universitè Pierre et Marie Curie
46. Noury S, Krokidis X, Fuster F, Silvi B (1999) Comput Chem 23:597
47. Flükiger P, Lüthi H-P, Portmann S, Weber J (2000) MOLEKEL 4.0. Swiss National Supercomputing Centre CSCS, Manno
48. Reed AE, Weinhold FJ (1985) Chem Phys 83:1736–1740
49. Reed AE, Curtiss LA, Weinhold F (1988) Chem Rev 88:899–926
50. Chesnut DB (2003) J Phys Chem A 107:4307
51. Chesnut DB (2001) Chem Phys 271:9
52. Sánchez-González A, Martínez-Garcia H, Melchor S, Dobado JA (2004) J Phys Chem A 108:9188
53. Chesnut DB (2000) Heterat Chem 11:341
54. Shaik S, Danovich D, Silvi B, Lauvergnat DL, Hiberty PC (2005) Chem Eur J 11:6358
55. Matito E, Silvi B, Duran M, Solà M (2006) J Chem Phys 125:024301
56. Lepetit C, Silvi B, Chauvin R (2003) J Phys Chem 107:464
57. Pilme J, Silve B, Alikhani ME (2005) J Phys Chem A 109:10028